VNU Journal of Science: Mathematics - Physics

Journal homepage: https://js.vnu.edu.vn/MaP

Original Article

Formation of Co_3O_4 Nanosheets or Nanorods: Effect of Experimental Condition

Dam Huy Dat[1,2], Le Thai Tuan Anh[1,2], Vu Nhat Hoa[1,2], Phan Quoc Thang[1,2], Nguyen Thi Tuyet Dung[1,2], Dang Thi Thanh Le[1,2,*]

[1]*School of Materials Science and Engineering (SMSE), Hanoi University of Science and Technology (HUST), 1 Dai Co Viet, Hanoi, Vietnam*

[2]*International Training Institute for Materials Science (ITIMS), Hanoi University of Science and Technology (HUST), 1 Dai Co Viet, Hanoi, Vietnam*

Received 27th January 2026
Revised 16th March 2026; Accepted 13th April 2026

Abstract: In this study, Co_3O_4 nanostructures were synthesized by hydrothermal method through a two-step process including hydrothermal followed by heat treatment. The hydrothermal conditions, such as temperature and time, were varied to obtain the morphological characteristics of the Co_3O_4 nanostructures. The morphological and structural characteristics were analyzed by techniques such as field-effect scanning electron microscopy (FESEM) and X-ray diffraction (XRD). Our findings reveal that the nanostructures exhibit diverse morphologies, depending on the hydrothermal conditions. In addition, we investigated the gas sensing capabilities of the nanosheets to ammonia.

Keywords: Co_3O_4, nanosheets, hydrothermal, gas sensor.

1. Introduction

Cobalt oxide (Co_3O_4) is an important transition metal oxide that exhibits magnetic behavior and p-type semiconducting characteristics, with reported direct optical band gaps of approximately 1.52 and 2.13 eV [1]. Owing to these properties, Co_3O_4 has attracted considerable interest for a wide range of applications, including supercapacitors [2], lithium-ion batteries [3, 4], and particularly gas sensing devices [5, 6]. Structurally, Co_3O_4 belongs to the spinel-type metal oxides, with a cubic phase being the most thermodynamically stable and commonly observed crystal structure [7]. To date, various wet-

* Corresponding author.
E-mail address: le.dangthithanh@hust.edu.vn / thanhle@itims.edu.vn

https//doi.org/10.25073/2588-1124/vnumap.5112

chemical synthesis strategies have been developed to fabricate Co_3O_4 nanostructures with diverse morphologies, such as nanoparticles [8], nanocubes [9], nanorods [10], nanotubes [11], nanowires [12], nanowalls [13], hollow polyhedrons [14], and hierarchical nanostructures [15-17].

Among these morphologies, two-dimensional (2D) Co_3O_4 nanostructures are particularly attractive for gas sensing applications due to their large specific surface area and high porosity. In general, 2D materials exhibit pronounced sensitivity to environmental changes, making them promising candidates for ultra-sensitive chemical sensors. Their unique layered architectures provide exceptionally high surface-to-volume ratios and abundant active sites, enabling enhanced gas adsorption, rapid charge transfer, low sensing noise, and high sensitivity. In particular, field-effect transistor (FET)-based chemical sensors, which are widely employed for 2D materials, offer additional advantages, including simple device configurations, low power consumption, and facile fabrication processes [18, 19].

Extensive efforts have been devoted to the synthesis of cobalt oxide nanostructures using techniques such as hydrothermal processing [20], electrospinning [21], chemical vapor deposition [1], sputtering [22] and pulsed laser deposition [23], among others. Nevertheless, many of these approaches require stringent conditions, including high temperatures, high vacuum environments, and complex processing steps, which increase fabrication costs and limit large-scale implementation. By contrast, hydrothermal synthesis has emerged as a highly attractive alternative due to its simplicity, low energy consumption, and scalability.

In this study, Co_3O_4 nanosheets were successfully synthesized via a surfactant-free hydrothermal method. The effects of hydrothermal reaction time and temperature on the morphology of the resulting Co_3O_4 nanostructures are systematically investigated.

2. Experimental

Urea ($CO(NH_2)_2$) and cobalt nitrate hexahydrate ($Co(NO_3)_2{\cdot}6H_2O$, ≥98%) were purchased from Sigma-Aldrich (Germany) and used as received without further purification.

Co_3O_4 nanosheets were synthesized via a simple hydrothermal method. In a typical procedure, appropriate amounts of cobalt nitrate hexahydrate and urea were dissolved in 50 mL of deionized water under vigorous magnetic stirring, resulting in a homogeneous pale pink solution. Continuous stirring was maintained for 5 min to ensure uniform dispersion of Co^{2+} ions. The resulting solution was then transferred into a 100 mL Teflon-lined stainless-steel autoclave, sealed, and heated at various temperatures (120, 140, and 200 °C) for different reaction durations (3, 14, 18 and 24 h).

After completion of the hydrothermal reaction, the precipitated products were collected by filtration, thoroughly washed with deionized water, and dried at 60 °C to obtain powder samples. The dried precursors were subsequently placed in an alumina boat and calcined in a tubular furnace at 600 °C for 2 h. Through the thermal decomposition of the pink–green precursor, which mainly consisted of cobalt hydroxide ($Co(OH)_2$) nanostructures, polycrystalline Co_3O_4 nanostructures were formed upon calcination (Fig. 1).

The as-prepared precursors and the calcined Co_3O_4 nanostructures were systematically characterized using X-ray diffraction (XRD), scanning electron microscopy (SEM), and energy-dispersive X-ray spectroscopy (EDS). XRD measurements were carried out on a Bruker D5005 diffractometer employing Cu $K\alpha_1$ radiation (λ = 1.5406 Å) operated at 40 kV and 40 mA. SEM images were acquired using a JEOL 7600 field-emission scanning electron microscope at an accelerating voltage of 10 kV.

The gas sensors were fabricated using a conventional thick-film technique. Co_3O_4 nanosheets were first dispersed in *N*-vinylpyrrolidone to form a homogeneous colloidal suspension. The resulting suspension was subsequently deposited onto a silicon substrate integrated with Pt interdigitated electrodes. The gas sensing characteristics of the fabricated sensor were evaluated using a custom-built

laboratory gas sensing measurement system. Prior to sensing measurements, the device was preheated at 500 °C for 2 h to improve film stability and interfacial adhesion. Electrical resistance measurements were performed using a Keithley 2602 source meter while the sensor was subjected to cyclic exposures of NH_3 in dry air. Gas concentrations (50–1000 ppm) were precisely metered using MKS GV50 mass flow controllers, with a constant total flow rate of 400 sccm. All gas-sensing tests were carried out at 50 °C in a bespoke measurement chamber. Sensor response was defined as $S = R_g/R_a$ where R_a and R_g denote the steady-state resistances in air and in the presence of the target gas, respectively [24, 25].

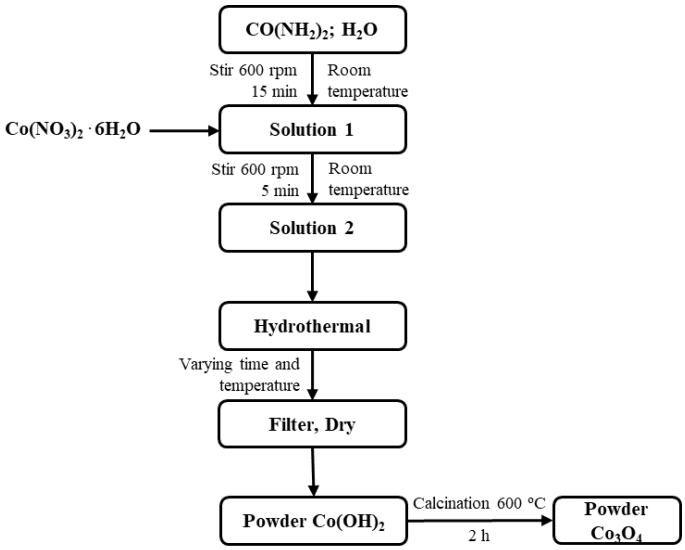

Figure 1. Preparation procedure of Co_3O_4 nanostructures at different times and temperatures.

3. Results and Discussion

3.1. Effect of Synthesis Time and Temperature

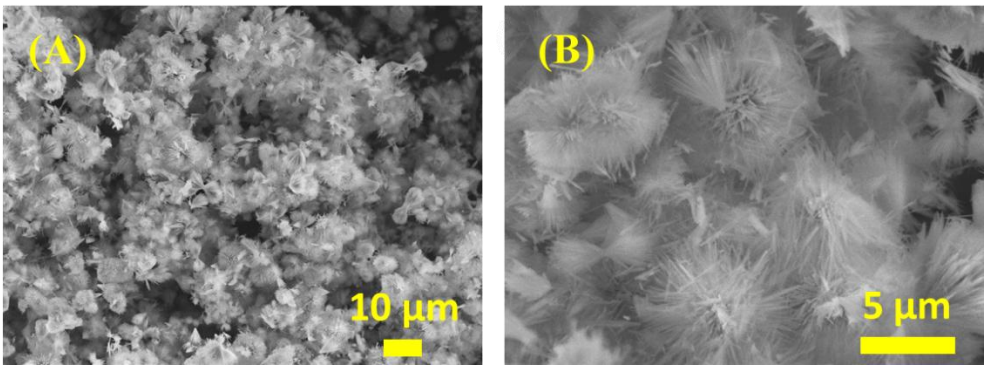

Figure 2. SEM images of as-prepared cobalt hydroxide carbonate nanostructure at 120 °C for 3 h at different magnifications: A) low magnification, B) high magnification.

The hydrothermal process was employed to regulate the morphology of the as-prepared cobalt hydroxide carbonate nanostructures, with the time and temperature acting as the controlling factors.

SEM images of the cobalt hydroxide carbonate nanorods synthesized at 120 °C for 3 hours, captured at various magnifications, are presented in Figure 2. The images indicate that the obtained material only composes nanorods which possess a diameter < 200 nm nanometers, with lengths varying between 2 and 5 micrometers.

Following the initial hydrothermal synthesis at 120 ℃ for 3 hours, the temperature was maintained, while the process time was extended up to 24 hours. The obtained product was characterized and displayed in Figure 3, which shows SEM images of the cobalt hydroxide carbonate nanosheets captured at different magnifications. The images reveal that the width of the nanosheets ranged from 500 to 700 nanometers, the length varied from 5 to 10 micrometers while the thickness is around of 50-100 nm. Notably, there is no nanorod morphology.

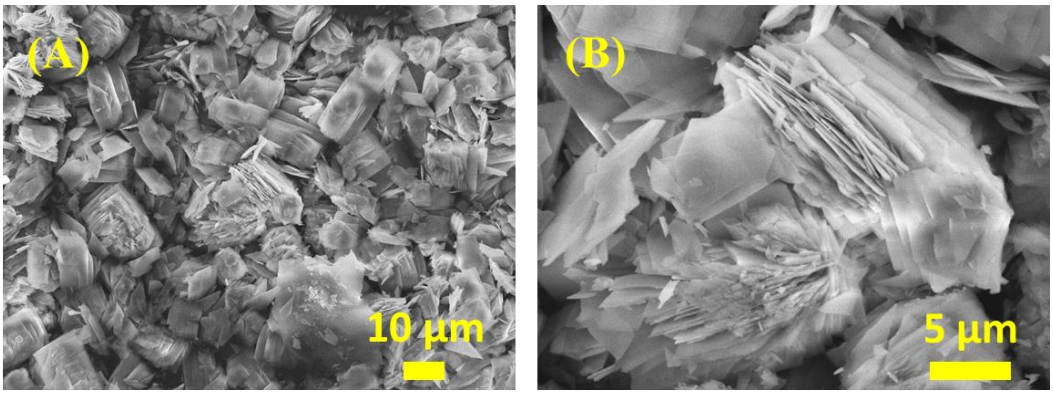

Figure 3. SEM images of as-prepared cobalt oxalate nanostructure at 120 °C for 24 h at different magnifications: A) low magnification, B) high magnification.

To investigate the impact of the hydrothermal temperature on the morphology of the cobalt hydroxide carbonate nanostructures, the hydrothermal time was held constant at 3 hours, while the process temperature was increased to 200 °C. The SEM images of the resulting cobalt hydroxide carbonate nanostructures synthesized at 200 °C for 3 hours are displayed in Figure 4.

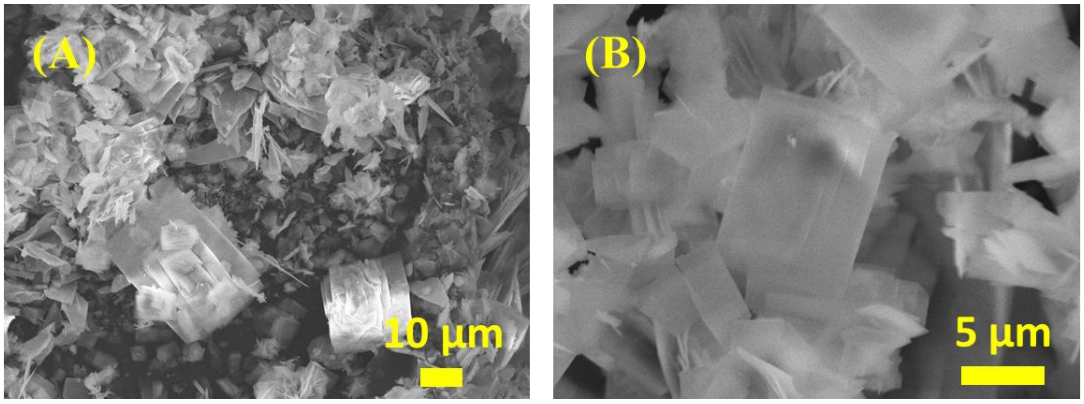

Figure 4. SEM images of as-prepared cobalt hydroxide carbonate nanostructure at 200 °C for 3 h at different magnifications: A) low magnification, B) high magnification.

It can be seen that the width of the nanosheets ranged from 500 to 700 nanometers, the length varied from 2 to 5 micrometers while the thickness is around of 50-100 nm. This condition resulted in ununiform nanosheets in comparison to those prepared at 120 °C/3 h (Fig. 2). There is no nanorod morphology at this synthesis condition as well.

Subsequently, the process temperature was maintained at 200 °C while the process time was extended to 24 hours. Under this condition, we obtained nanosheets that were long in length but small in width, possessing a clear border. The SEM images of the synthesized nanosheets captured at various magnifications are presented in Figure 5. The obtained nanosheets were not uniform, with a diameter ranging from 200-800 nm and lengths varying between 2-20 µm, much larger than those at the other preparation conditions.

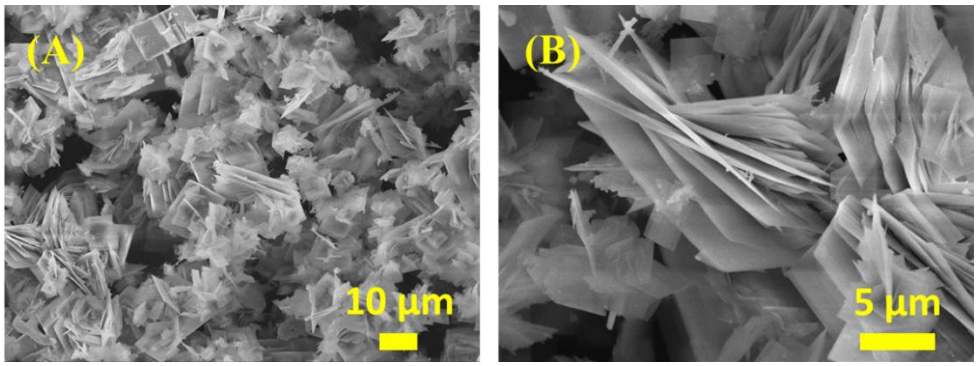

Figure 5. SEM images of as-prepared cobalt oxalate nanostructure at 200 °C for 24 h at different magnifications: A) low magnification, B) high magnification.

Then time of the hydrothermal process were set at 18 h while the temperature was kept at 140 °C. At this condition of synthesis, morphology of nanosheet was domination with uniformity, as shown in Figure 6.

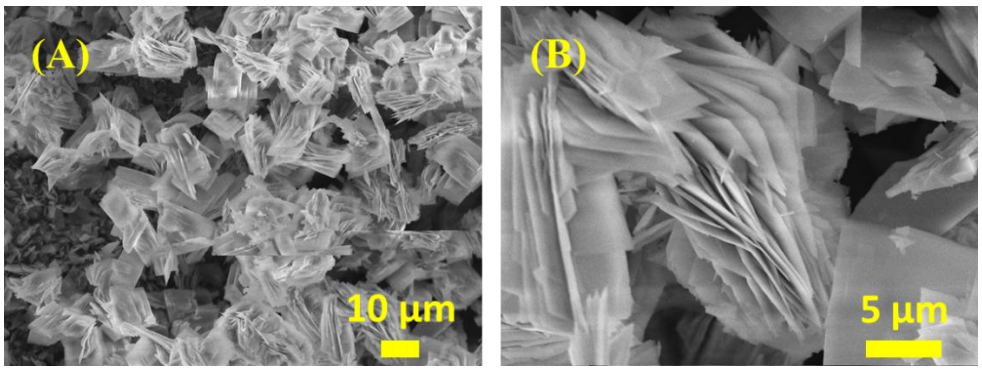

Figure 6. SEM images of as-prepared cobalt hydroxide carbonate nanosheets at 140 °C for 18 h at different magnifications: A) low magnification, B) high magnification.

Therefore, after investigating effect of time and temperature of synthesis process on morphology of nanostructures, it is transparent to confirm that 140 °C/18 h is the best condition to achieve uniform nanosheets with narrow width. This condition of synthesis was chosen for further characterizations in the current study.

3.2. Composition and Structural Properties

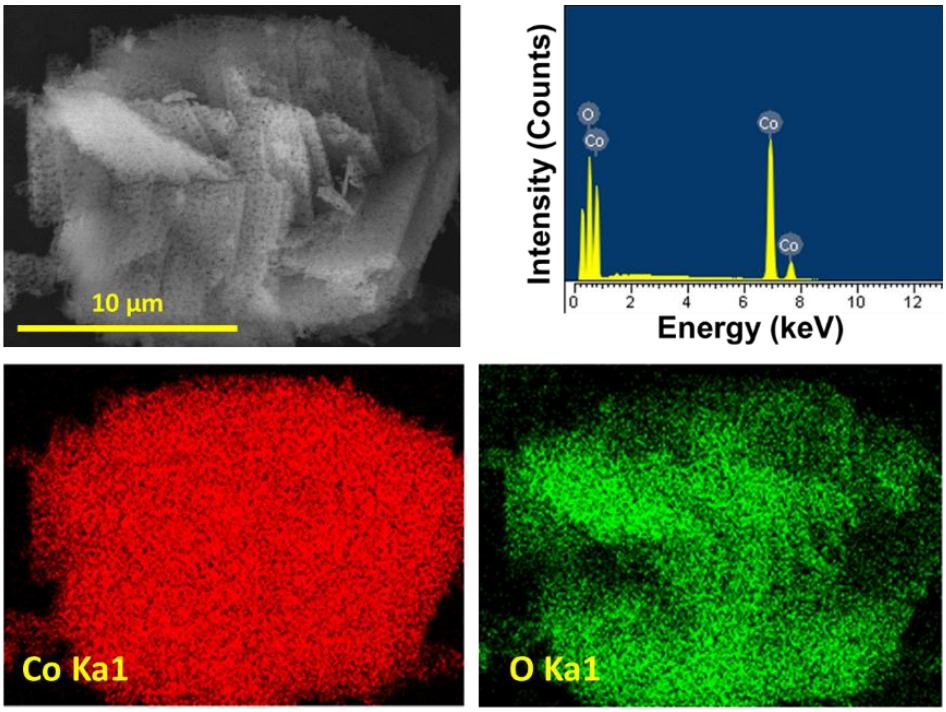

Figure 7. a) EDS spectrum and b) EDS mapping of cobalt oxide nanosheets prepared at 140 °C for 18 h.

The elemental composition of the annealed sample was investigated by energy-dispersive X-ray spectroscopy (EDS) and elemental mapping analyses. The EDS spectrum shown in Fig. 7a confirms the presence of cobalt (Co) and oxygen (O) as the constituent elements of the as-prepared sample. Moreover, the corresponding EDS elemental mapping images (Fig. 7b) reveal a homogeneous spatial distribution of Co and O across the entire Co_3O_4 nanosheets, indicating good compositional uniformity of the cobalt oxide nanosheets.

Fig. 8 presents the X-ray diffraction (XRD) patterns of the precursor nanosheets obtained after hydrothermal treatment at 140 °C for 18 h and the corresponding cobalt oxide nanosheets after subsequent calcination at 500 °C for 2 h. The XRD pattern of the as-prepared precursor, as shown in Fig. 8(A), exhibits characteristic diffraction peaks. These reflections can be indexed to the (020), (130), (040), (140), (031), and (240) crystallographic planes of monoclinic cobalt hydroxide carbonate, $Co_2(OH)_2CO_3$, in good agreement with the standard JCPDS card No. 29-1416, confirming the successful formation of the precursor phase during the hydrothermal process.

After thermal treatment at 500 °C, the XRD patterns of the resulting samples display a set of well-defined diffraction peaks located at 2θ values of 31.4°, 36.9°, 44.9°, 59.4°, and 65.3°, which are indexed to the (220), (311), (400), (511), and (440) planes of cubic spinel Co_3O_4 (JCPDS card No. 42-1467) (Fig. 8B). No impurity-related peaks are observed, indicating the complete conversion of the precursor into phase-pure Co_3O_4 upon calcination. Notably, the (311) reflection exhibits the highest intensity for all calcined samples, suggesting preferential crystal growth along this crystallographic direction. Furthermore, the pronounced enhancement in the intensity of the diffraction peak at 36.9° compared to that of the hydrothermally synthesized precursor provides additional evidence for improved crystallinity and the successful formation of Co_3O_4 following heat treatment.

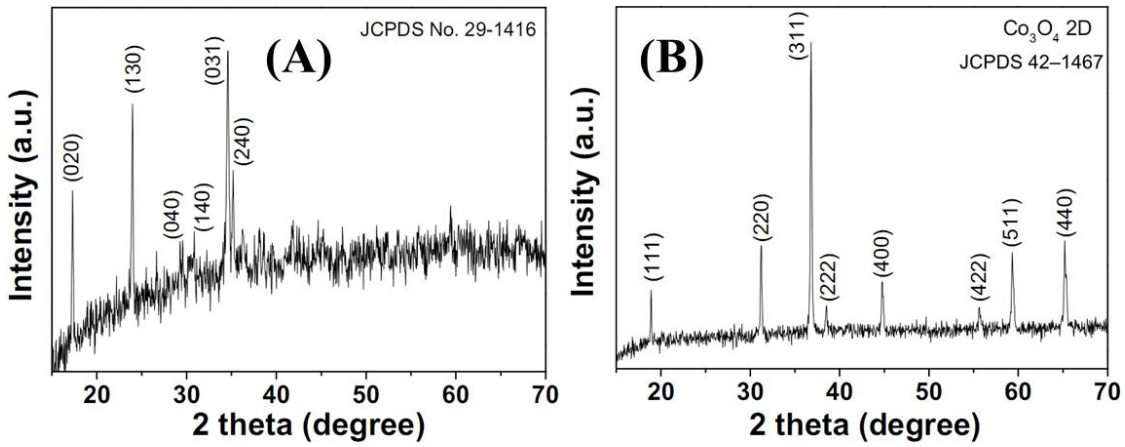

Figure 8. A) XRD of as-prepared cobalt hydroxide carbonate nanosheets at 140 °C/18 h and cobalt oxide nanosheets annealed at 500 °C.

3.3. Gas Sensing Property

The Co_3O_4 nanosheets synthesized under hydrothermal conditions at 140 °C for 18 h and subsequently annealed at 500 °C for 2 h were selected for the investigation of ammonia sensing performance. The dynamic resistance response of the Co_3O_4-based sensor was evaluated at various operating temperatures (250, 300, 350, 400, and 450 °C) and NH_3 concentrations ranging from 50 to 1000 ppm. The corresponding sensing characteristics are summarized in Fig. 9, providing a comprehensive assessment of the NH_3 sensitivity of the Co_3O_4 nanosheets.

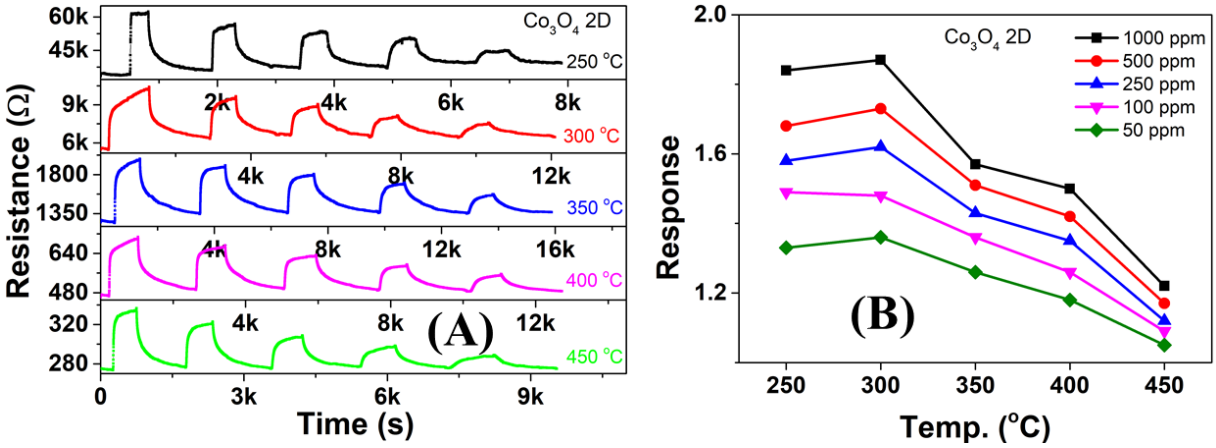

Figure 9. Response to NH_3 of the Co_3O_4 sensor prepared at 140 °C/18 h: (a) Transient resistance verse response time to 50–1000 ppm at various working temperatures 250 °C – 450 °C, (b) Response to diverse concentrations 50–1000 ppm at different temperatures 250 °C – 450 °C.

Figure 9a presents the real-time resistance response curves of the Co_3O_4 nanosheet sensor measured at different operating temperatures. Upon exposure to NH_3 gas, the sensor resistance increases rapidly and subsequently returns to its baseline value after removal of the target gas, confirming the typical p-type semiconducting behavior of Co_3O_4. The sensing results further reveal a pronounced dependence of

the baseline resistance on the operating temperature, with the background resistance increasing as the temperature decreases. Specifically, the baseline resistance is approximately 34000 Ω at 250 °C and increases significantly to about 270 Ω at 450 °C.

Figure 9b presents the sensor response derived from the dynamic resistance curves shown in Figure 9a. At an operating temperature of 300 °C, the Co_3O_4 nanosheet-based sensor exhibits its highest response (S = 1.87) toward 1000 ppm NH_3. Meanwhile, the corresponding responses are 1.73, 1.62, 1.48, and 1.36 at different concentrations of 500, 250, 100 and 25 ppm, respectively. These results clearly indicate that the sensor response increases with increasing NH_3 concentration. Notably, in the low-concentration regime, the sensor demonstrates a higher response at 300 °C compared to other operating temperatures, suggesting that 300 °C represents the optimal working temperature when considering both sensitivity and stability. Overall, the Co_3O_4 nanosheet sensor exhibits its best sensing performance at an operating temperature of 300 °C.

Co_3O_4 is a well-known p-type semiconductor under typical preparation conditions. Its gas sensing is fundamentally rooted in the surface-governed chemiresistive effect, a process where the electrical resistance of the material changes in response to the checmical composition of the surrounding atmosphere. As a p-type semiconductor, the electrical conductivity of Co_3O_4 is primarily dominated by the movement of holes, which act as positive charge carriers. When the sensor is initially exposed to ambient air, oxygen molecules from the environment undergo an adsorption process onto the active surface of the nanosheets. These molecules capture free electrons from the semiconductor to become ionized into chemisorbed oxygen species, such as O^- and O_2^- according to the following reaction:

$$O_2 + e^- \rightarrow O_2^- \quad (1)$$

This electron sequestration leads to a significant increase in hole concentration within the Co_3O_4, effectively creating a “hole accumulation layer” near the surface which lowers the overall electrical resistance of the device. The transition to the sensing phase occurs when the material is exposed to NH_3, which acts as a reducing agent. Upon contact with the sensor surface, the NH_3 molecules undergo a redoc reaction with the previously chemisorbed oxygen species. This chemical interaction triggers the release of the trapped electrons back into the semiconductor, thereby reducing the hole concentration within the nanosheets. As a consequence, the Co_3O_4 lattice, as described by the following reaction:

$$2NH_3 + 3/2O_2^- \rightarrow N_2 + 3H_2O + 3/2e^- \quad (2)$$

After these returning electrons recombine with the majority charge carriers (the holes), they effectively reduce the hole concentration within the nanosheets. This modulation of charge carriers increases the potential barrier for electronic transport, resulting in a measurable and significant increase in the sensor's electrical resistance. The high sensitivity observed in this study is largely attributed to the nanosheet morphology, which provides an exceptionally high surface-to-volume ratio. This structural advantage maximizes the available sites for gas-solid interactions, thereby ensuring a rapid and robust transducer response to even low concentrations of ammonia.

4. Conclusion

This study reports the hydrothermal synthesis of Co_3O_4 nanostructures and systematically investigates the effects of reaction time and temperature on their structural evolution. Among the examined conditions, hydrothermal treatment at 140 °C for 18 h yielded well-defined Co_3O_4 nanosheets with optimized morphology. The gas sensing performance of the synthesized Co_3O_4 nanosheets toward NH_3 was subsequently evaluated. The sensor based on Co_3O_4 nanosheets demonstrated its highest sensing response to NH_3 at an optimal operating temperature of 300 °C, highlighting the strong potential of these nanostructures for ammonia gas sensing applications.

Acknowledgments

This research is funded by Hanoi University of Science and Technology (HUST) under project number T2025-PC-109.

References

[1] A. Gulino, P. Dapporto, P. Rossi, I. Fragalà, A Novel Self-generating Liquid MOCVD Precursor for Co_3O_4 Thin Films, Chemistry of Materials, Vol. 15, 2003, pp. 3748-3752, https://doi.org/10.1021/cm034305z.

[2] W. Guo, X. Lian, Y. Tian, T. Yang, S. Wang, Facile Fabrication 1D/2D/3D Co_3O_4 Nanostructure in Hydrothermal Synthesis for Enhanced Supercapacitor Performance, Journal of Energy Storage, Vol. 38, 2021, pp. 102586, https://doi.org/10.1016/j.est.2021.102586.

[3] F. Zhan, B. Geng, Y. Guo, Porous Co_3O_4 Nanosheets with Extraordinarily High Discharge Capacity for Lithium Batteries, Chemistry-A European Journal, Vol. 15, 2009, pp. 6169-6174, https://doi.org/10.1002/chem.200802561.

[4] Y. Ren, X. Xiao, J. Ni, H. Zhao, H. Yang, X. Chen, RuO_2 Incorporated Co_3O_4 Nanosheets as Carbon-free Integrated Cathodes for Lithium-oxygen Battery Application, Materials Letters, Vol. 304, 2021, pp. 130634, https://doi.org/10.1016/j.matlet.2021.130634.

[5] H. Nguyen, S. A. E. Safty, Meso- and Macroporous Co_3O_4 Nanorods for Effective VOC Gas Sensors, The Journal of Physical Chemistry C, Vol. 115, 2011, pp. 8466-8474, https://doi.org/10.1021/jp1116189.

[6] P. L. Quang, N. D. Cuong, T. T. Hoa, H. T. Long, C. M. Hung, D. T. T. Le, N. V. Hieu, Simple Post-synthesis of Mesoporous p-Type Co_3O_4 Nanochains for Enhanced H_2S Gas Sensing Performance, Sensors Actuators B: Chemical, Vol. 270, 2018, pp. 158-166, https://doi.org/10.1016/j.snb.2018.05.026.

[7] K. J. Kormondy, A. B. Posadas, A. Slepko, A. Dhamdhere, D. J. Smith, K. N. Mitchell, T. I. W. Gies, S. Zollner, L. G. Marshall, J. Zhou, A. A. Demkov, Epitaxy of Polar Semiconductor Co_3O_4 (110): Growth, Structure, and Characterization, Journal of Applied Physics, Vol. 115, 2014, pp. 243708, https://doi.org/10.1063/1.4885048.

[8] P. G. Choi, T. Fuchigami, K. I. Kakimoto, Y. Masuda, Effect of Crystal Defect on Gas Sensing Properties of Co_3O_4 Nanoparticles, ACS Sensors, Vol. 5, 2020, pp. 1665-1673, https://doi.org/10.1021/acssensors.0c00290.

[9] A. Ma, S. Y. Baek, J. H. Seo, S. A. Abbas, J. H. Kwon, S. J. Ahn, K. M. Nam, Photodeposition of Pt Nanoparticles on Co_3O_4 Nanocubes for Detection of Acetone at Part-Per-Billion Levels, ACS Applied Nano Materials, Vol. 4, 2021,pp. 2752-2759, https://doi.org/10.1021/acsanm.0c03393.

[10] T. T. L. Dang, T. N. T. Do, V. M. Do, M. Tonezzer, V. D. N. Tran, T. X. Chu, M. H. Chu, V. D. Nguyen, D. H. Nguyen, Eco-friendly Facile Synthesis of Co_3O_4–Pt Nanorods for Ethylene Detection towards Fruit Quality Monitoring, Sensors Actuators A: Physical, Vol. 362, 2023, pp. 114607, https://doi.org/10.1016/j.sna.2023.114607.

[11] Z. Fei, S. He, L. Li, W. Ji, C. T. Au, Morphology-directed Synthesis of Co_3O_4 Nanotubes Based on Modified Kirkendall Effect And Its Application in CH_4 Combustion, Chemical Communications, Vol. 48, 2012, pp. 853-855, https://doi.org/10.1039/C1CC15976C.

[12] Y. Sun, P. Lv, J. Y. Yang, L. He, J. C. Nie, X. Liu, Y. Li, Ultrathin Co_3O_4 Nanowires with High Catalytic Oxidation of CO, Chemical Communications, Vol. 47, 2011, pp. 11279-11281, https://doi.org/10.1039/c1cc14484g.

[13] L. Xiong, Y. Teng, Y. Wu, J. Wang, Z. He, Large-scale Synthesis of Aligned Co_3O_4 Nanowalls on Nickel Foam and Their Electrochemical Performance for Li-ion Batteries, Ceramics International, Vol. 40, 2014, pp. 15561-15568, https://doi.org/10.1016/j.ceramint.2014.07.032.

[14] Y. Zhang, Y. Wu, Z. Duan, B. Liu, Q. Zhao, Z. Yuan, S. Li, J. Liang, Y. Jiang, H. Tai, High Performance Humidity Sensor Based on 3D Mesoporous Co_3O_4 Hollow Polyhedron for Multifunctional Applications, Applied Surface Science, Vol. 585, 2022, pp. 152698, https://doi.org/10.1016/j.apsusc.2022.152698.

[15] J. Cao, S. Wang, J. Li, Y. Xing, X. Zhao, D. Li, Porous Nanosheets Assembled Co_3O_4 Hierarchical Architectures for Enhanced BTX (Benzene, Toluene and Xylene) Gas Detection, Sensors Actuators B: Chemical, Vol. 315, 2020, pp. 128120, https://doi.org/10.1016/j.snb.2020.128120.

[16] Z. Zhang, Y. Song, J. Sun, Self-stacked $Co(OH)_2/Co_3O_4$ Nanosheets for High-selectivity Gas Sensor to N-butyl Alcohol, Applied Surface Science, Vol. 610, 2023, pp. 155438, https://doi.org/10.1016/j.apsusc.2022.155438.

[17] J. Deng, R. Zhang, L. Wang, Z. Lou, T. Zhang, Enhanced Sensing Performance of The Co_3O_4 Hierarchical

Nanorods to NH_3 Gas, Sensors Actuators B: Chemical, Vol. 209, 2015, pp. 449-455, https://doi.org/10.1016/j.snb.2014.11.141.

[18] C. Wang, Y. Song, M. Zhao, H. Lu, J. Wang, X. Zou, Material Design and Mechanism Interpretation of Metal Oxide Nanofibers for Improving Gas Sensitivity, Coordination Chemistry Reviews, Vol. 531, 2025, pp. 216492, https://doi.org/10.1016/j.ccr.2025.216492.

[19] M. Hjiri, N. Benmansour, F.M. Barakat, G. Neri, Metal Oxide Gas Sensors with Nanosheet Morphology: A Review, Microchemical Journal, Vol. 215, 2025, pp. 114510, https://doi.org/10.1016/j.microc.2025.114510.

[20] Y. Qiu, Y. Wang, Controllable Synthesis of Porous Co_3O_4 Nanorods and Their Ethanol-sensing Performance, Ceramics International, Vol. 48, 2022, pp. 29659-29668, https://doi.org/10.1016/j.ceramint.2022.06.221.

[21] D. T. T. Le, V. A. Tuan, M. Tonezzer, C. M. Hung, N. D. Hoa, An Electrospinning Deposited Cobalt Oxide Nanofiber Gas Sensing Device: Selective Enhancement as A Thermal Electronic Nose, RSC Advances, Vol. 15, 2025, pp. 15293-15301, https://doi.org/10.1039/d5ra00873e.

[22] R. Hippler, M. Cada, P. Ksirova, J. Olejnicek, P. Jiricek, J. Houdkova, H. Wulff, A. Kruth, C.A. Helm, Z. Hubicka, Deposition of Cobalt Oxide Films by Reactive Pulsed Magnetron Sputtering, Surface and Coatings Technology, Vol. 405, 2021, pp. 126590, https://doi.org/10.1016/j.surfcoat.2020.126590.

[23] H. Y. Kwong, Y. W. Wong, Formation of Cobalt Hydroxide Single-crystal Platelets from Pulsed Laser Deposited Cobalt Thin Film, Journal of Alloys and Compounds, Vol. 497, 2010, pp. 267-271, https://doi.org/10.1016/j.jallcom.2010.03.024.

[24] L. V. Duy, T.T. Nguyet, D.T.T. Le, N. V. Duy, H. Nguyen, F. Biasioli, M. Tonezzer, C. Di Natale, N.D. Hoa, Room Temperature Ammonia Gas Sensor Based on p-Type-like V_2O_5 Nanosheets towards Food Spoilage Monitoring, Nanomaterials, Vol. 13, 2023, pp. 146, https://doi.org/10.3390/nano13010146.

[25] D. H. Yen, L. T. N. Phu, D. T. T. Le, Synthesis of Tungsten Oxide Nanofibers Using Electrospinning Towards Gas Sensor Application, VNU Journal of Science: Mathematics - Physics, Vol. 41, No. 2, 2025, pp. 84-91, https://doi.org/10.25073/2588-1124/vnumap.4993.